

# A Gravitational Wave Detector for Post-Merger Neutron Stars: Beyond the Quantum Loss Limit of Michelson Fabry–Pérot Interferometer

Teng Zhang,<sup>1, 2, 3</sup> Huan Yang,<sup>4, 5</sup> Denis Martynov,<sup>1</sup> Patricia Schmidt,<sup>1</sup> and Haixing Miao<sup>6, 7</sup>

<sup>1</sup>*School of Physics and Astronomy, and Institute for Gravitational Wave Astronomy, University of Birmingham, Edgbaston, Birmingham B15 2TT, United Kingdom*

<sup>2</sup>*Department of Gravitational Waves and Fundamental Physics, Maastricht University, 6200 MD Maastricht, The Netherlands*

<sup>3</sup>*Nikhef, Science Park 105, 1098 XG Amsterdam, The Netherlands*

<sup>4</sup>*Perimeter Institute for Theoretical Physics, Waterloo, Ontario N2L 2Y5, Canada*

<sup>5</sup>*University of Guelph, Guelph, Ontario N1G 2W1, Canada*

<sup>6</sup>*Department of Physics, Tsinghua University, Beijing, China*

<sup>7</sup>*Frontier Science Center for Quantum Information, Beijing, China*

Advanced gravitational-wave detectors that have made groundbreaking discoveries are Michelson interferometers with resonating optical cavities as their arms. As light travels at finite speed, these cavities are optimal for enhancing signals at frequencies below their bandwidth frequency. A small amount of optical loss will, however, significantly impact the high-frequency signals which are not optimally amplified. We find an elegant interferometer configuration with an “L-resonator” as the core, significantly surpassing the loss limited sensitivity of dual-recycled-Fabry–Pérot–Michelson interferometers at high frequencies. Following this concept, we provide a broadband design of a 25 km detector with outstanding sensitivity between 2–4 kHz. We have performed Monte-Carlo population studies of binary neutron star mergers, given the most recent merger rate from the GWTC-3 catalog and several representative neutron star equations of state. We find that the new interferometer configuration significantly outperforms other third-generation detectors by a factor of 3 to 7 in the signal-to-noise ratio of the post-merger signal. Assuming a detection threshold with signal-to-noise ratio  $> 5$  and for the cases we have explored, the new design is the only detector that confidently achieves a detection rate larger than one per year, with the rate being 1 to 30 events per year.

## I. INTRODUCTION

In 2015, the first direct detection of gravitational waves was made by the Laser Interferometer Gravitational-Wave Observatory (LIGO) [1]. Since then, gravitational waves have become a new window for observing the universe and probing the unexplored territories in astrophysics, cosmology and fundamental physics. Until now, more than 90 compact binary merger events have been confidently observed by the network of advanced detectors including Virgo and KAGRA [2]. Within these events, the detection of a binary neutron star coalescence, GW170817 [3] followed shortly by a short gamma-ray burst, GRB 170817A [4] and the a series of joint observations of electromagnetic counterparts [5] have had profound scientific impacts: This multi-messenger discovery confirmed that binary neutron star mergers are the origin of at least some short gamma-ray bursts and a production site for heavy elements via rapid neutron-capture [5]. In the cosmology aspect, GW170817 has led to an independent measurement of the Hubble constant [6]. It also provided unique access to probe the internal structure of neutron stars and their equation of state by constraining their tidal deformability [3, 7–11]. With both gravitational wave and gamma ray measurements, new constraints/bounds have been placed on the speed of gravitational waves and the violation of Lorentz invariance, in addition to a new test of the equivalence principle [4].

Current gravitational wave detectors are only sensitive to the inspiral part of binary neutron star mergers, as shown in the analysis of GW170817. The post-merger gravitational wave signal, which concentrates in the kilo-hertz band, encodes essential information to answer many important questions, *e.g.* the origin(s) of heavy element nucleosynthesis, the engine of gamma-ray jets and the inner structure of the neutron star under extreme conditions. In particular, the merger and post-merger signals provide the access to completely unexplored regimes in the Quantum Chromodynamics phase diagram beyond the reach of terrestrial collision experiment [12], where novel phase of matter may appear, *e.g.* from hadron-quark phase transition [13–15].

The successful performance of current gravitational wave detectors relies on their Michelson-type design. In addition to the canonical Michelson interferometer configuration, extra mirrors have been introduced in the arms to form Fabry–Pérot cavities which boost both the optical power and the gravitational wave signals, giving so called Fabry–Pérot–Michelson (FPMI) interferometer [16]. With these modifications, the shot noise, arising from the quantum statistics of photons, is suppressed by orders of magnitude within the cavity bandwidth, which is typically from a few hertz to tens of hertz.

On the other hand, the binary neutron stars post-merger signals are mainly between 2 to 4 kilohertz which is beyond the optimal band of current gravitation wave detectors. To better explore the neutron star physics,

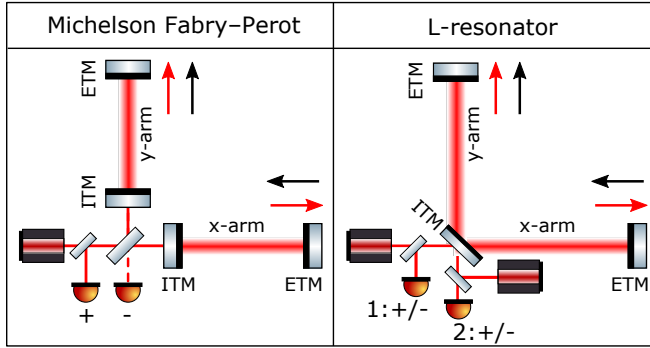


FIG. 1. Schematic of FPMI interferometer and the "L-resonator". They are both sensible to two degrees of freedoms of motion: naming common, "+", mode indicated by red arrows and differential, "-", mode (gravitational wave mode) indicated by black arrows.

there are various ideas developed to improve the high-frequency sensitivity of the modern and future detectors based on the dual-recycled-Fabry-Pérot-Michelson (DRFPMI) interferometer, which includes power recycling cavity at the bright port and signal recycling cavity/signal extraction cavity (SEC) at the dark port to further enhance the arm cavity power and adjust the detectors response [17, 18]. One straightforward approach is to make usage of the adjustability of SEC which forms a coupled system with arm cavity. For example, the signal resonant frequency of the detector can be shifted to higher frequencies by constant SEC detuning [19] or exploring the SEC-arm coupled cavity resonance [20–22]. More sophisticated quantum schemes, including the white light cavity [23–28] and the nonlinear optical parametric amplifier [29], aim at broadening the effective bandwidth of the detector without sacrificing its peak sensitivity, hence overcoming the Mizuno limit [30]. However, it is the optical loss that sets a universal and ultimate sensitivity limit of a quantum detector [31]. The schemes mentioned above for improving the high-frequency sensitivity are all severely constrained by the optical losses in the SEC, which directly attenuate the signal emerging from the arm cavity. Even worse, the SEC loss limited high frequency sensitivity is independent from the arm length. Several studies have been carried out to explore various techniques to saturate or overcome the SEC loss limit [32, 33]. It has been realised that a sloshing-type Sagnac configuration can beat the SEC loss limit by adding a filter cavity between two arms and thus shaping coupled cavity resonances in the absence of SEC. However, the filter cavity loss becomes the new limiting factor as another internal loss [33]. Physically the intrinsic limit of high frequency sensitivity comes from the decay of signal beyond the bandwidth of the single cavity where the signal is generated and circulates around.

In order to surpass the loss limit of gravitational wave detectors at high frequencies, the question becomes whether it is possible to resonate high frequency sig-

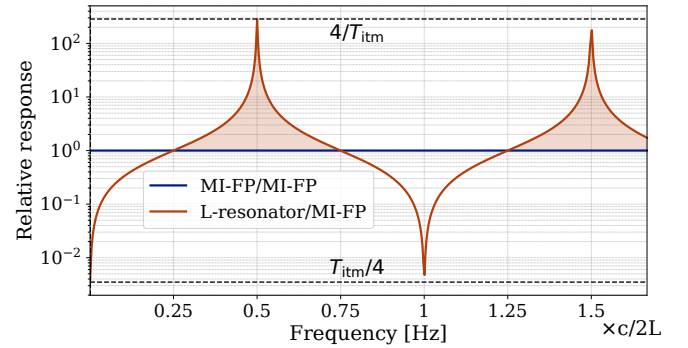


FIG. 2. The relative response of the "L-resonator" and FPMI interferometer to the differential mode. The "L-resonator" outperforms at  $c/4L$  and  $3c/4L$  with a relative amplification of  $4/T_{itm}$ , where  $T_{itm}$  is chosen as 0.014. In contrast, the FPMI interferometer outperforms around frequency 0 Hz and  $c/2L$ .

nals in the arm cavity by itself, and in the meanwhile, the laser carrier needs to resonate to maintain the high power. This motivates the idea of taking the advantage of resonance at free spectral range away from the carrier frequency [34]. However, the detector's response to gravitational waves largely degrades around the free spectral range frequency (zero for waves at normal incidence) [35–37].

In this paper, we provide an elegant detector scheme satisfying all criteria. The SEC loss limited lower bound sensitivity of the new detector can in principle be orders of magnitude better than that of DRFPMI interferometer at high frequencies. A conceptual design of the new detector including all other losses surpasses the quantum loss limit of currently proposed gravitational waves detectors by several times. In Sec. II, we introduce the principle of the core of new detector, an "L-resonator". In Sec. III, we present the full interferometer and its quantum noise. In Sec. IV, we deliver the conceptual design of the new detector and model the noise budget. In Sec. V, we demonstrate the ability of the new detector to detect the post-merger signal of binary neutron star coalescence and dark matter induced neutron star collapse.

## II. PRINCIPLE

To illustrate the principle of the new scheme, we start from the fundamental of FPMI interferometer. Here, we define two orthogonal degrees of freedom of motions: the common, "+", and differential, "-", motions of end test masses (ETMs) in x- and y-arms,

$$\Delta L_+ = \Delta L_x + \Delta L_y, \Delta L_- = \Delta L_x - \Delta L_y. \quad (1)$$

The differential mode signal transmits to dark port and common mode signal appears at bright port. The interferometer's responses to the sidebands of both modes are

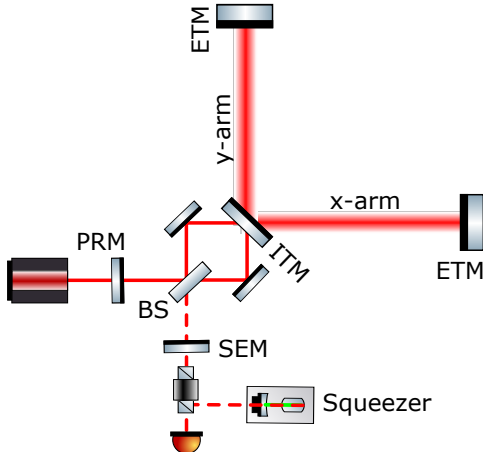


FIG. 3. The schematic of new interferometer comprised of the “L-resonator” and a central Michelson. It also includes power recycling cavity (PRM) and signal extraction cavity (SEM). Constant phase squeezing is injected from the dark port.

identical and proportional to

$$G_{\text{FPMI},+/-} = \frac{\sqrt{2T_{\text{itm}}}}{|e^{2i\Omega\tau} - \sqrt{R_{\text{itm}}}|}, \quad (2)$$

where  $\Omega$  is the angular frequency of sideband,  $\tau \equiv L/c$ ,  $L$  is the arm length,  $T_{\text{itm}}$  and  $R_{\text{itm}}$  are the transmissivity and reflectivity of input test mass (ITM).

We propose an “L-resonator” as shown in Fig. 1. Such a resonator responds the two modes of motions in different manners, giving separated resonant frequency. The phase variation of light after a round trip in the cavity is  $\Delta\phi(t) = (2\omega_0/c)[\Delta L_x(t - 2\tau) + \Delta L_y(t)]$ , which, in the frequency domain, can be written as

$$\Delta\phi(\Omega) = \frac{2\omega_0}{c}(1 \pm e^{-2i\Omega\tau})\Delta L_{\pm}(\Omega). \quad (3)$$

$\omega_0$  is the angular frequency of the carrier. It is clear that when  $\Omega/2\pi = Nc/2L$  ( $N$  is an integer), the phase shift of “+” mode reaches maximum, in contrast, the “-” mode peaks at  $\Omega/2\pi = Nc/2L + c/4L$ . Here we pump the resonator by two lasers from both input ports, which give balanced power in the two orthogonal arms [38]. The signal of both modes of motions will appear at both ports as indicated in Fig. 1. The responses of the two ports to the “+” and “-” mode are proportional to

$$G_{L,1,+} = G_{L,2,+} = \frac{\sqrt{T_{\text{itm}}}}{|e^{2i\Omega\tau} - \sqrt{R_{\text{itm}}}|}, \quad (4)$$

$$G_{L,1,-} = -G_{L,2,-} = \frac{\sqrt{T_{\text{itm}}}}{|e^{2i\Omega\tau} + \sqrt{R_{\text{itm}}}|}.$$

By combining and splitting the “+” and “-” mode signal at two ports, we can tell the “L-resonator” has an identical “+” mode response to that of FPMI interferometer. Regarding to the “-” mode, “L-resonator” has

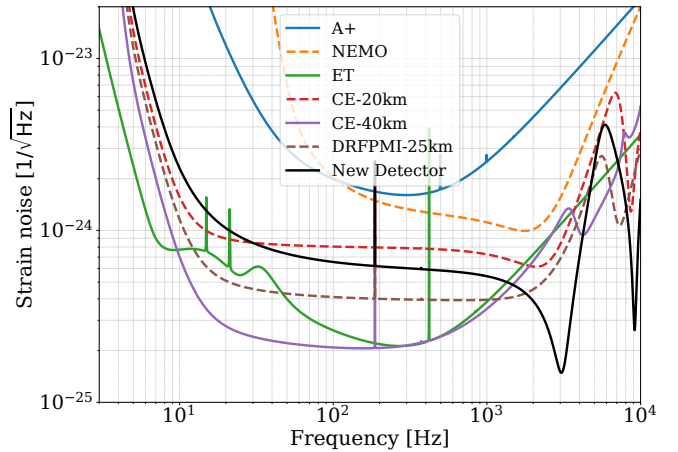


FIG. 4. Strain sensitivity of the 25 km new detector in comparison to A+ [39, 40], NEMO [21], ET [41], the so called “post-merger” tuned CE-20 km and the CE-40 km [42, 43] detectors. The sensitivity of ET corresponds to the combined three 10 km triangular configurations. The DRFPMI-25 km is a “post-merger” tuned design of DRFPMI interferometer with equivalent parameters to the new detector. The new detector gives superior sensitivity in the frequency range of 2-4 kHz and 8-10 kHz. The parameters of the new detector are listed in Table I. I.

$4/T_{\text{itm}}$  times larger response at  $c/4L$ , as shown in Fig. 2. The expense is around  $\Omega = 0$  and  $c/2L$ . It is worth of noting that, at  $\Omega = 0$ , the response is not zero as one may infer directly from Eq. 3.

How about its response to gravitational waves? Treating the ITM and ETM in x-arm/y-arm of the “L-resonator” as the boundary of photon’s trajectory in two directions, the round trip phase in one direction under the projection of gravitational waves is exactly the same as in the Michelson interferometer where the beamsplitter (BS) and ETM form the boundary [36]. By calculating the optical field after traveling through the whole cavity, it turns out regarding the cavity’s response, the strain of normal incident waves can be mapped to an equivalent differential displacement as follows

$$\Delta L_{-}(\Omega) = L \frac{\sin \Omega\tau}{\Omega\tau} h(\Omega), \quad (5)$$

which is the same as that of the Michelson interferometer [35-37]. It is clear that only at multiples of  $c/2L$ , instead of  $c/4L$ , the gravitational wave corresponds to 0 effective displacement. This conclusion is not surprising, as by treating the effect of both gravitational wave and mirror displacement as the modulation of the phase of light, their equivalent relation should be independent from the optical response of the system to the sidebands.

### III. THE COMPLETE INTERFEROMETER AND QUANTUM NOISE

Each output port of the “L-resonator” is sensitive to both common and differential modes. We can decouple the two modes of signals through electronic system after measuring their signals. More practically, we can use a single laser and add a BS to form the complete interferometer as shown in Fig. 3, which decouples the two modes spatially. In Fig. 3, the sideband extraction mirror (SEM) and power recycling mirror (PRM) are also included. Note that in the lossless case, the laser travels in and returns back along the same input port, and the reflection port turns out to be a dark port. The BS therefore behaves more like the one in the Michelson instead of the Sagnac interferometer as what the topology might indicate. The SEM helps to decrease the storage-time of the sidebands around  $c/4L$ , therefore broaden the detector bandwidth [30]. In contrast, it increases the low frequency sidebands storage time, which refers to the signal recycling scheme in DRFPMI interferometer [17, 30]. A similar high frequency resonance can be achieved by the synchronous interferometer [44–47], which uses a ring cavity as its core. It realises a speed-type measurement which suppresses the signals at low frequencies. The new interferometer is a position meter which is also sensitive to signals towards DC.

The quantum noise of the new interferometer can be derived following the conventional approach of modelling the field propagation in the interferometer. The single sided quantum noise power spectral density of the interferometer in the unit of  $\text{m}^2/\text{Hz}$  is

$$S(\Omega) = \frac{c^2 \hbar |e^{2i\Omega\tau} + \sqrt{R_{\text{sec}}}|^2}{4\omega_0 P_{\text{arm}} T_{\text{sec}}} + \frac{16\hbar\omega_0 P_{\text{arm}} T_{\text{sec}}}{c^2 M^2 |e^{2i\Omega\tau} + \sqrt{R_{\text{sec}}}|^2 \Omega^4}, \quad (6)$$

$M$  is the mass of each ETM. Here  $R_{\text{sec}}$  and  $T_{\text{sec}}$  are the effective reflectivity and transmissivity of the SEC formed by ITM and SEM:

$$T_{\text{sec}} \equiv \frac{T_{\text{itm}} T_{\text{sem}}}{[1 - \sqrt{R_{\text{itm}} R_{\text{sem}}}]^2}, \quad (7)$$

where  $T_{\text{sem}}$ ,  $R_{\text{sem}}$  are the power transmissivity and reflectivity of SEM. More precisely, we include the additional phase gained by the sidebands propagating in the SEC, there is

$$S(\Omega) = \frac{c^2 \hbar |\mathcal{C}|^2}{4\omega_0 P_{\text{arm}} T_{\text{itm}} T_{\text{sem}}} + \frac{16\hbar\omega_0 P_{\text{arm}} T_{\text{itm}} T_{\text{sem}}}{c^2 M^2 |\mathcal{C}|^2 \Omega^4} \quad (8)$$

where

$$\mathcal{C} = e^{2i\Omega(\tau+\tau_s)} + \sqrt{R_{\text{itm}}} \left[ e^{2i\Omega\tau_s} - e^{2i\Omega\tau} \sqrt{R_{\text{sem}}} \right] - R_{\text{sem}}. \quad (9)$$

Here  $\tau_s \equiv L_{\text{sec}}/c$ ,  $L_{\text{sec}}$  is the SEC length. The first term of Eq. (8) is the shot noise,  $S_{\text{shot}}$ , the second term denotes the radiation pressure noise. The power spectral density

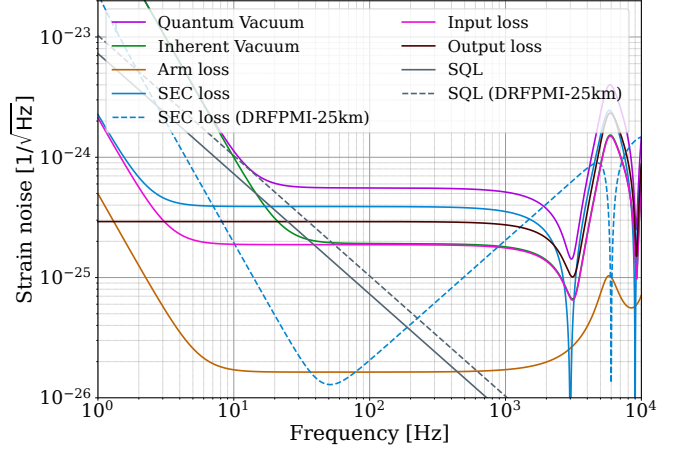


FIG. 5. Detailed quantum noise budget of the new detector. At 3 kHz, the SEC loss limit of new detector is orders of magnitude lower than that of the equivalent DRFPMI detector. The quantum noise of new detector is limited by the output loss. The amplitude spectral density of the standard quantum limit of the new detector is  $\sqrt{2}$  lower than that of an equivalent DRFPMI detector.

of the SEC loss can be calculated as

$$S_{\text{sec}}(\Omega) = \epsilon_{\text{sec}} \left[ \frac{c^2 \hbar |e^{2i\Omega\tau} + \sqrt{R_{\text{itm}}}|^2}{4\omega_0 P_{\text{arm}} T_{\text{itm}}} + \frac{16\hbar\omega_0 P_{\text{arm}} T_{\text{itm}}}{c^2 M^2 |\mathcal{C}|^2 \Omega^4} \right] \quad (10)$$

where  $\epsilon_{\text{sec}}$  is the SEC loss coefficient. The power spectral density of the input loss is  $S_{\text{in}}(\Omega) = \epsilon_{\text{in}} S(\Omega)$ , where  $\epsilon_{\text{in}}$  is the input loss coefficient. The power spectral density of the output loss is  $S_{\text{out}}(\Omega) = \epsilon_{\text{out}} S_{\text{shot}}(\Omega)/(1 - \epsilon_{\text{out}})$ , where  $\epsilon_{\text{out}}$  is the output loss coefficient. The arm loss power spectral density can be calculated as

$$S_{\text{arm}}(\Omega) = \epsilon_{\text{arm}} \left[ \frac{c^2 \hbar}{8\omega_0 P_{\text{arm}}} + \frac{8\hbar\omega_0 P_{\text{arm}} |e^{2i\Omega\tau_s} - \sqrt{R_{\text{itm}} R_{\text{sem}}}|^2}{c^2 M^2 |\mathcal{C}|^2 \Omega^4} \right], \quad (11)$$

where  $\epsilon_{\text{arm}}$  is the arm coefficient.

### IV. CONCEPTUAL DESIGN AND NOISE BUDGET

Targeting at the post-merger signals of binary neutron stars, typically between 2-4 kHz, we propose a detector with each arm length 25 km, which results peak sensitivities at 3 kHz. The sensitivities of the new detector, Advanced LIGO+ (A+) [39, 40], Neutron Star Extreme Matter Observatory (NEMO) [21] Einstein Telescope (ET) [41] and Cosmic Explorer (CE) [42, 43] are compared in the Fig. 4.

### A. Interferometer design

In such a detector, we choose laser wavelength at 1064 nm and fused silica as the mirror material, same as in LIGO and Virgo detectors [39, 48]. We target the arm cavity power, 4 MW, which can be obtained with 500 W input laser and 100 ppm round trip arm cavity loss (equivalent to 50 ppm loss in each arm cavity of the DRFPMI interferometer). On the conceptual level, we reasonably assume other power degradation mechanisms, *e.g.* the point absorbers on the surface of optics [49], the parametric acousto-optic coupling [50] will be manageable in the future benefiting from both optimising detector's technical design and future research and development. The ITM transmissivity is chosen as 0.014. The SEM transmissivity is chosen as 0.06 and SEC length is chosen as 100 m. The resulting detector bandwidth is  $\sim 290$  Hz.

The radius of curvature of two ETMs are chosen to be 36 km (cavity g factor  $\sim 0.15$ ), resulting beam size of 13.6 cm on ETMs. The beam is elliptical on the ITM, with size of 7.5 and 10.6 cm in two axis ( $10.6 \text{ cm} = \sqrt{2} \times 7.5 \text{ cm}$ , where 7.5 cm is the waist size). We adopt the mirror radius and thickness both 36 cm, which gives total weight  $\sim 322$  kg. Here the ratio of mirror radius over beam size is chosen to be  $> 2.63$  to keep the clipping loss  $< 1$  ppm. In the new detector, the displacement of ITM along its normal is in the common mode, the sub-optimal geometry of the ITM which leads larger mirror thermal fluctuations [51] is not a constrain from the noise perspective. We choose the ITM radius, 36 cm and thickness, 18 cm, giving mirror mass 161 kg. The coating material of ITM should have low optical absorption to reduce the heat load, hence reduce the optical loss in the recycling cavity from the thermal distortion [52] but is not required to have low mechanical loss, which is necessary to have by the ITMs in the DRFPMI interferometer.

### B. Radiation pressure noise and squeezing

In the new detector, there are only two ETMs that contribute to the effective differential mode, which is half reduced compared with that of DRMIFP interferometer. Equivalently, the reduced mirror mass of the differential mode is a factor of 2 larger, hence the quantum radiation pressure amplitude noise is reduced by a factor of 2. It is straightforward to read that Eq. (8) reaches the minimum value when the shot noise and the radiation pressure noise are equal:

$$S(\Omega) \geq \frac{4\hbar}{M\Omega^2}, \quad (12)$$

which is the power spectral density of the standard quantum limit of the new interferometer. It is only half of the standard quantum limit of a DRMIFP interferometer [54].

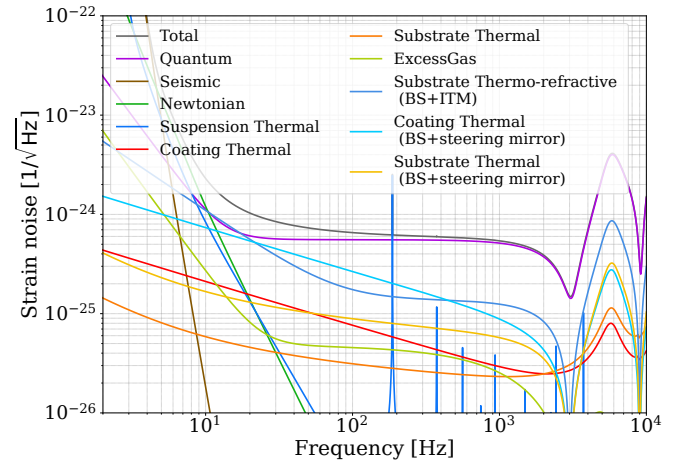


FIG. 6. Noise budget of the 25 km new detector. Above 20 Hz, the sensitivity of the new detector is limited by quantum shot noise. Instead of frequency dependent squeezing, only constant phase squeezing is applied. The seismic noise. Newtonian noise and suspension thermal noise include both arm cavity and central Michelson noise. We present the BS and ITM coating and substrate noise separately. The noise budget is modelled by the software, pyGWINC [53].

TABLE I. Parameters of the 25 km new detector

Wavelength	1064 nm
Arm length	25 km
SEC length	100 m
Input laser power	500 W
Power recycling cavity power	29 kW
Arm circulating power	4 MW
ITM transmissivity	0.014
SRM transmissivity	0.06
Arm loss	100 ppm
SEC loss	1000 ppm
Input loss	1.5%
Output loss	3.5%
Input squeezing level	18 dB
Result squeezing (shot noise)	9-11.5 dB
Result squeezing (radiation pressure noise)	-15 dB
Substrate material	Silica
ITM/ETM mass	161/322 kg
ITM radius/thickness	36 cm/18 cm
ETM radius/thickness	36 cm/36 cm
ITM/ETM RoC	$\infty$ / 36 km
ITM/ETM beam size	7.5 cm / 13.6 cm
BS radius/thickness	36 cm/18 cm
BS beam size	7.5 cm
Coating loss angle (ETM/steering mirror)	9e-5/1.25e-5

Benefiting from the naturally reduced radiation pressure noise, we only adopt constant phase squeezing instead of frequency dependent squeezing. As a result, the usual kilo-meter long filter cavity is not required. We assume 18 dB constant phase squeezing can be generated. The loss projection on the input path is 1.5%, including 1% from the optical parametric amplifier and 0.5% from

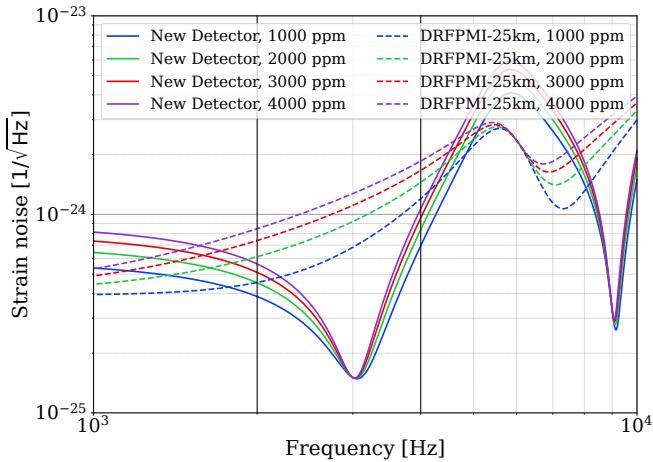


FIG. 7. Sensitivity comparison between the proposed new detector and an equivalent “post-merger” tuned DRFPMI configuration having SEC loss from 1000 to 4000 ppm.

Faraday isolator. Note here the input loss budget is less than the estimation in other third generation detectors, where filter cavity is required on the input chain. Such projection will result 15 dB squeezing into the interferometer and give 15 dB amplification of radiation pressure noise. The output path including Faraday isolator (0.5%), output mode cleaner (2%) and the photodiodes (1%), contribute total 3.5% loss [55]. Including the internal loss from SEC (1000 ppm) and arm cavity (100 ppm), 9-11.5 dB squeezed shot noise will be observed over the whole frequency band, with 11.5 dB squeezing at the peak sensitivity. The detailed quantum noise compositions are shown in Fig. 5.

### C. Arm cavity noise

The arm cavity effective mirror displacement noises are reduced compared with equivalent DRFPMI interferometer, again benefiting from the in-susceptibility to ITM motions.

We modelled the noise budget of the new detector using software pyGWINC [53]. The noise modelling is based on the CE-40 km design [56]. For the coating thermal Brownian noise modelling, we assume a factor 4 improvement from the mechanical loss of  $Ta_2O_5$  and  $SiO_2$  bi-layer coatings, which is also the goal of A+ [40]. The ETM suspension design is assumed to be the quadrupole pendulum suspension used in LIGO [56, 57]. The vertical seismic and suspension thermal noise has the least coupling due to the finite radius of curvature of the earth and are independent from arm length in the unite of strain. They will scale down by  $\sqrt{2}$  from CE-40 km. The horizontal seismic and suspension thermal noise will scale up by 1.13 ( $40/25/\sqrt{2}$ ). Newtonian noise is also around a factor of 1.13 times the CE-40 km noise. The residual gas noise caused by the stochastic disturbance of molecular

species onto the laser’s phase [58] is not mirror displacement noise and will almost scale up by 1.6 ( $40/25$ ). The gas damping noise, however, from the impinging of the gas particles onto test masses [59, 60] will scale up by 1.13.

### D. Central Michelson noise

Different from the DRFPMI interferometer, where the central Michelson noise is attenuated by the arm cavity buildup factor, the optical paths fluctuations in the central Michelson of the new detector is non-negligible at low frequency and around  $c/2L$  due to the anti-resonance of the arm cavity in those frequency bands. The power spectral density of the Michelson differential noise can be mapped to the equivalent ETM noise as

$$S_{etm}(\Omega) = S_{MI}(\Omega) \frac{|e^{2i\Omega\tau} + \sqrt{R_{itm}}|^2}{4}, \quad (13)$$

where  $S_{MI}(\Omega)$  is the central Michelson noise and  $S_{etm}(\Omega)$  is thus the detection noise. Such fundamental noise can largely come from the the change of the refractive index of the BS and ITM substrate due to inhomogeneous temperature fluctuations, so called substrate thermo-refractive noise [61–63]. The central Michelson thermo-refractive noise coming from both BS and ITM substrate can be calculated by Equation (2) in [62] including elliptical beam corrections. The beam size on BS will be almost the same as on the ITM. We chose the BS geometry the same as the ITM with 36 cm radius and 18 cm thickness.

We also include the suspension, coating and substrate thermal noise from the BS and the two steering mirrors between the BS and the ITM. The folding mirror gives two times coherent mirror displacement noise in a round trip. It also introduces larger mirror thermal noise in each bounce compared with a straight reflection due to the interference fringe pattern [64, 65]. It is 50% addition in power spectral density for coating Brownian noise [64, 65], the dominated thermal noise. The coating of steering mirrors have the same mechanical loss as that of the ETMs. For the seismic noise and seismic Newtonian noise of the central Michelson, the scale of the central Michelson should be smaller than the wavelength of the seismic waves, the motions of Michelson mirrors can be largely coherent as a certain mix of differential and common modes. For the simplicity, we just assume uncorrelated noise from each mirror. The seismic isolation systems of central Michelson mirrors are the same as these of the ETMs. The detailed noise budget of the new detector is shown in Fig. 6.

### E. Equivalent DRFPMI detector

The current and third generation detectors based on DRFPMI interferometer have separate design with different baseline parameters, which are also different from

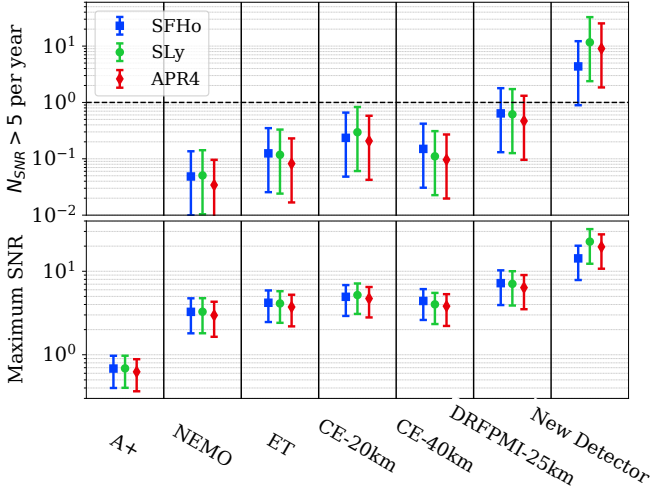


FIG. 8. Number of events with SNR greater than five (top) and the SNR of the loudest event (bottom), both assuming one year of observing time. They are obtained from the median values in the Monte-Carlo simulations. The upper ends of the error bars correspond to the case with the merger rate being  $295.7 \text{Gpc}^{-3} \text{yr}^{-1}$ , the lower ends correspond to  $21.6 \text{Gpc}^{-3} \text{yr}^{-1}$  and the symbols correspond to  $105.5 \text{Gpc}^{-3} \text{yr}^{-1}$ .

the parameters choices of the new detector in this paper. To deliver an unbiased comparison of the DRFPMI and the new “L-resonator” interferometer, we present a DRFPMI detector with equivalent parameters of the new detector. Such a DRFPMI interferometer based detector has arm length 25 km, arm cavity power 4 MW and 18 dB squeezing with 3% loss on the input path and 3.5% loss on the output path. The filter cavity for frequency dependent squeezing in the DRFPMI interferometer contribute 1.5% more input loss compared with the new detector. The interferometer is tuned for post-merger neutron stars [42, 43]. The classical noise modeling are based on CE design. With different assumptions of SEC loss, the sensitivities of the new detector and the DRFPMI-25 km detector are shown in Fig. 7. Within the concerned frequency band for post-merger neutron stars, *i.e.* 2-4 kHz, the performance of the DRFPMI-25 km detector is highly SEC loss dependent, while the new detector is robust from SEC loss contamination. The full band sensitivity is shown in Fig. 4.

## V. SCIENCE CASES

The new configuration leads to a broadband sensitivity as shown in Fig. 4, hence such a detector will still be able to probe the astrophysics of compact binaries and cosmology similar to third-generation detectors (see e.g. [66]), though with modified signal-to-noise ratios (SNRs). In this section we highlight two specific science cases that become accessible due to the unparalleled sensitivity at high frequencies offered by the new design.

### A. Neutron star post-merger

The primary science target of this new detector design is the post-merger gravitational wave signal of coalescing binary neutron star systems. While the ringdown spectroscopy of binary black hole coalescences provides a novel platform for tests of General Relativity [67–70], the post-merger spectroscopy of binary neutron stars will likely shed light on our understanding of the equation of state of nuclear matter at high temperatures, complicated magnetohydrodynamical processes involving neutrino generation and transport, novel phase(s) of nuclear matter and the underlying mechanism of short gamma-ray bursts [71–79].

The post-merger waveform of binary neutron stars is a complicated (and unknown) function of the neutron star masses, spins and the equation of state. We perform an analysis similar to the one presented in [20] and choose three representative equations of state: SFHo [80], SLy [81] and APR4 [82] to cover a range of different stiffness. The neutron star binary is assumed to be  $1.35M_{\odot} + 1.35M_{\odot}$ , and the corresponding waveforms are adopted from [80, 82–86]. We assume the updated binary neutron star merger rate after the third observing run of the Advanced LIGO-Virgo detector network,  $105.5^{+190.2}_{-83.9} \text{Gpc}^{-3} \text{yr}^{-1}$  [87]. We note that it is an order of magnitude smaller than the initial rate estimated after the detection of GW170817 [3] (and used in [20]). For each of the three equations of states, we apply Monte-Carlo simulations to randomly sample binary neutron stars in their sky locations, inclinations and distances according to the merger rate, assuming one-year of observation time and a uniform distribution of binaries in comoving volume. We repeat this exercise 100 times to generate 100 universes with the same underlying distribution but different statistical realization. We compute the post-merger SNR for each event, defined as

$$\text{SNR} := 2 \sqrt{\int_{f_{\text{contact}}}^{4\text{kHz}} df \frac{|\tilde{h}(f)|^2}{S_n(f)}}, \quad (14)$$

where  $\tilde{h}$  is the frequency-domain post-merger waveform,  $S_n(f)$  is the single sided noise power spectral density of the considered detector, and  $f_{\text{contact}}$  is the frequency at neutron stars collide with each other [83, 88], which depends on the equation of state. It can be computed from the mass ratio of the binary and the compactness of the neutron stars [88]. The upper cut-off frequency is chosen to be 4 kHz to cover most of the spectral power of the post-merger waveform. We note that this is a slightly different definition of the post-merger SNR than the one used in [43, 89], where instead of  $f_{\text{contact}}$  a fixed lower cut-off frequency of 1 kHz is used. Here we choose the equation-of-state dependent contact frequency as we are not considering the part of the post-merger spectrum that overlaps with inspiral frequencies. The resulting median number of events with a post-merger SNR  $> 5$  and the median SNR of the loudest event, averaged over

the 100 realisations and assuming three different merger rates, are shown in Fig. 8. We find that the new design significantly outperforms – by a factor of 3 to 7 – other third-generation detectors in detecting the post-merger signal of colliding neutron stars. If the detection threshold is chosen to be  $\text{SNR} > 5$ , then only the new design is confidently expected to observe at least one event per year, whereas the detection rates for NEMO, ET and CE are one-to-two orders of magnitude smaller. Notice that here the SNR is defined for the total post-merger waveform, which is greater than the SNR stemming from the excitation of individual oscillation modes of the post-merger object. Therefore, the new design provides the most promising platform to perform post-merger spectroscopy, i.e., resolving the “peak mode” and other secondary oscillation modes of the remnant [90].

### B. Dark Matter Induced Neutron Star Collapse

In addition to the prominent sensitivity between 2-4 kHz, the new detector also has significant sensitivity between 8-10 kHz. In this section, we study its potential advantage for even higher frequency science case.

It has been proposed that fermionic dark matter particles may accumulate at the center of neutron stars and eventually collapse to a mini black hole because of the dissipative interaction. The neutron star matter subsequently accrete onto the mini black hole in millisecond timescale and produce gravitational wave emission in the kHz range, depending on the mass of the collapsing neutron star.

For a rotating neutron star the primary gravitational wave signal is the 20 mode of the axisymmetric collapse. The collapse waveform is discussed in [91], which displays similar magnitude (in  $\psi_4$ ) as the collapse waveform of hypermassive neutron star as used in [34]. For simplicity we shall use the phenomenological waveform model in [34] to compute the signal-to-noise ratio of these events:

$$h = A \frac{50\text{Mpc}}{d} \sin(2\pi f t) e^{-\pi f |t|/Q} \quad (15)$$

with the pre-peak part contributing comparable SNR as the post-peak part. Here the mode frequency is inversely proportional to mass  $f \sim 4.7\text{kHz} \times (2.7M_\odot/M_{\text{NS}})$ , the quality factor is  $Q \sim 2.5$  and the amplitude is estimated as  $A \sim 0.8 \times 10^{-23} (4.7\text{kHz}/f)^2$  (assuming the “TM1” equation of state). Notice that these values are expected to change for various neutron star spin and equation of state. For example, the amplitude may change by at least a factor of three according to the equation of states used in [91], and the variation of frequency and quality factor may be  $\leq 30\%$  or  $\leq 20\%$  respectively [34].

As shown in Fig. 9, with the waveform model of the collapse process, we can estimate the horizon distance if the detection threshold is set to be  $\text{SNR} = 5$ . The new design shows approximately a factor of 1.5 improvement in horizon distance over the entire mass range comparing

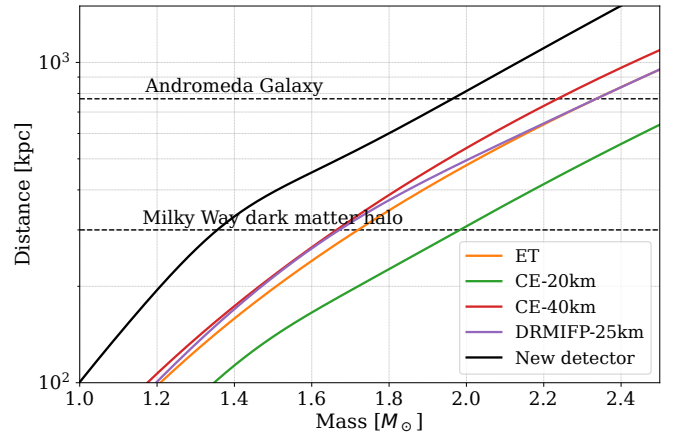


FIG. 9. Horizon distance for detecting the dark-matter induced neutron star collapse signal with different detector sensitivities, assuming the threshold SNR is 5.

with other third-generation detectors and the equivalent DRFPMI detector. For neutron star mass around 1.4 solar mass, the improvement is around a factor of 2, benefiting the secondary dip in the sensitivity curve of the new detector Fig. 4. The enhanced horizon distance allows to reach the edge of Milky Way’s dark matter halo for low mass collapse events and Andromeda Galaxy and its satellite galaxies in a larger mass range.

## VI. CONCLUSION

As an extraordinary laboratory to study the nuclear physics, the post-merger neutron stars call the demand of enhancing the gravitational wave detectors sensitivity in kilohertz band. The currently existing and proposed gravitational wave detector are based on DRFPMI interferometer. Since the Fabry–Pérot cavity is limited to have a narrow bandwidth to maintain its high finesse operation, such configurations have sub-optimal performance toward high frequencies. The fundamental limit comes from the optical loss, in particular, the loss in the SEC which mixes with decayed high frequency signals from the arm cavity sets the barrier.

In this work, we present an elegant interferometer based on a “L” shape optical resonator, which allows to amplify the high frequency gravitational wave signals and carrier in the meantime. The SEC loss limited sensitivity of such an interferometer surpasses that of a DRFPMI interferometer by orders of magnitude at high frequencies, more precisely,  $4/T_{\text{itm}}$  at  $c/4L$ . Beyond its high frequency superiority, its in-susceptibility to the ITM motion provides a factor of  $\sqrt{2}$  suppression of the arm cavity mirror displacement noises and a factor of 2 suppression of the quantum radiation pressure noise. It also brings other advantages, for example, the constant phase squeezing turns out to be sufficient; the ITM coatings only require to satisfy low optical absorption without demanding low

mechanical loss. The drawback of the new interferometer is at low frequencies around 0 Hz, where the noises in the central Michelson couple to the detector readout with same gain of arm cavity noise. On the technical level, the potential topics of the parametric instability of the arm cavity [50], radiation pressure induced angular instability of the arm cavity [92] and required thermal compensation system [52] that will be different from the DRFPMI interferometer require separate study in the future.

We apply the sensitivity of new detector to measure its ability to detect the binary neutron star post-mergers through the Monte-Carlo population simulation. Based on the chosen equation of state, the new detector has SNRs a factor of 3 to 7 of the other third generation detectors. Taking the  $\text{SNR} > 5$  as the threshold and given the merger rate ranging from  $21.6 \text{ Gpc}^{-3} \text{ yr}^{-1}$  to  $295.7 \text{ Gpc}^{-3} \text{ yr}^{-1}$  according to GWTC-3 catalog, the new detector can enable a detection rate ranging from 1 to 30 per year.

In addition, we explored the potential advantage of the new detector on its ability to detect the dark matter induced neutron star collapse. Benefiting from the conspicuous sensitivity between 8-10 kHz, which results from the second resonance of the new interferometer at  $3c/4L$ , it gives additional  $\sim 30\%$  improvement for 1.4 solar mass neutron stars on top of a factor of 1.5 broadband improvement, in comparison to the horizon reach of other

configurations.

## VII. ACKNOWLEDGEMENTS

We thank LVK collaboration, Kevin Kuns, Daniel Brown, Mikhail Korobko, Jennifer Wright, Stefan Danilishin, Stefan Hild and Sebastian Steinlechner for fruitful discussions. T. Z., D. M., P. S. and H. M. acknowledge the support of the Institute for Gravitational Wave Astronomy at the University of Birmingham, STFC Quantum Technology for Fundamental Physics scheme (Grant No. ST/T006609/1), and EPSRC New Horizon Scheme (Grant No. EP/V048872/1). T. Z. acknowledges the support of department of Gravitational Waves and Fundamental Physics in Maastricht University and E-TEST project. H. M. is supported by State Key Laboratory of Low Dimensional Quantum Physics and the start-up fund from Tsinghua University. D. M. is supported by the 2021 Philip Leverhulme Prize. H. Y. is supported by the Natural Sciences and Engineering Research Council of Canada and in part by Perimeter Institute for Theoretical Physics. Research at Perimeter Institute is supported in part by the Government of Canada through the Department of Innovation, Science and Economic Development Canada and by the Province of Ontario through the Ministry of Colleges and Universities. P. S. acknowledges support from STFC Grant No. ST/V005677/1.

---

[1] T. L. S. Collaboration and T. V. Collaboration, *Phys. Rev. Lett.* **116**, 61102 (2016).

[2] R. Abbott, T. Abbott, F. Acernese, K. Ackley, C. Adams, N. Adhikari, R. Adhikari, V. Adya, C. Affeldt, D. Agarwal, et al., arXiv preprint arXiv:2111.03606 (2021).

[3] B. P. Abbott, R. Abbott, T. D. Abbott, et al. (LIGO Scientific Collaboration and Virgo Collaboration), *Phys. Rev. Lett.* **119**, 161101 (2017).

[4] B. P. Abbott, R. Abbott, T. D. Abbott, F. Acernese, K. Ackley, C. Adams, T. Adams, P. Addesso, R. X. Adhikari, V. B. Adya, and et al., *Astrophys. J. Lett.* **848**, L13 (2017), arXiv:1710.05834 [astro-ph.HE].

[5] L. S. Collaboration and V. Collaboration., *The Astrophysical Journal* **848**, L12 (2017).

[6] T. L. S. Collaboration and T. V. Collaboration, *Nature* **551**, 85 (2017).

[7] B. P. Abbott et al. (LIGO Scientific, Virgo), *Phys. Rev. Lett.* **121**, 161101 (2018), arXiv:1805.11581 [gr-qc].

[8] B. P. Abbott et al. (LIGO Scientific, Virgo), *Phys. Rev. X* **9**, 011001 (2019), arXiv:1805.11579 [gr-qc].

[9] B. P. Abbott et al. (LIGO Scientific, Virgo), *Class. Quant. Grav.* **37**, 045006 (2020), arXiv:1908.01012 [gr-qc].

[10] K. Chatziioannou, *Gen. Rel. Grav.* **52**, 109 (2020), arXiv:2006.03168 [gr-qc].

[11] Z. Pan, Z. Lyu, B. Bonga, N. Ortiz, and H. Yang, *Phys. Rev. Lett.* **125**, 201102 (2020), arXiv:2003.03330 [astro-ph.HE].

[12] C. Schmidt and S. Sharma, *Journal of Physics G: Nuclear and Particle Physics* **44**, 104002 (2017).

[13] N. Yasutake, T. Maruyama, and T. Tatsumi, *Phys. Rev. D* **80**, 123009 (2009).

[14] E. R. Most, L. J. Papenfort, V. Dexheimer, M. Hanuske, S. Schramm, H. Stöcker, and L. Rezzolla, *Phys. Rev. Lett.* **122**, 061101 (2019).

[15] A. Bauswein, N.-U. F. Bastian, D. B. Blaschke, K. Chatziioannou, J. A. Clark, T. Fischer, and M. Oertel, *Phys. Rev. Lett.* **122**, 061102 (2019).

[16] R. Drever, in *AIP Conference Proceedings*, Vol. 96 (American Institute of Physics, 1983) pp. 336–346.

[17] D. E. McClelland, *Australian Journal of Physics* **48**, 953 (1995).

[18] A. Buonanno and Y. Chen, *Phys. Rev. D* **67**, 062002 (2003).

[19] D. Ganapathy, L. McCuller, J. G. Rollins, E. D. Hall, L. Barsotti, and M. Evans, *Phys. Rev. D* **103**, 022002 (2021).

[20] D. Martynov, H. Miao, H. Yang, F. H. Vivanco, E. Thrane, R. Smith, P. Lasky, W. E. East, R. Adhikari, A. Bauswein, A. Brooks, Y. Chen, T. Corbitt, A. Freise, H. Grote, Y. Levin, C. Zhao, and A. Vecchio, *Phys. Rev. D* **99**, 102004 (2019).

[21] K. Ackley, V. B. Adya, P. Agrawal, P. Altin, G. Ashton, M. Bailes, E. Baltinas, A. Barbui, D. Beniwal, C. Blair, and et al., *Publications of the Astronomical Society of Australia* **37**, e047 (2020).

[22] J. Eichholz, N. A. Holland, V. B. Adya, J. V. van Heijningen, R. L. Ward, B. J. J. Slagmolen, D. E. McClelland, and D. J. Ottaway, *Phys. Rev. D* **102**, 122003 (2020).

[23] A. Wicht, K. Danzmann, M. Fleischhauer, M. Scully, G. Müller, and R. Rinkleff, *Optics Communications* **134**, 431 (1997).

[24] M. Zhou, Z. Zhou, and S. M. Shahriar, *Phys. Rev. D* **92**, 082002 (2015).

[25] H. Miao, Y. Ma, C. Zhao, and Y. Chen, *Phys. Rev. Lett.* **115**, 211104 (2015).

[26] J. Bentley, P. Jones, D. Martynov, A. Freise, and H. Miao, *Phys. Rev. D* **99**, 102001 (2019).

[27] M. A. Page, M. Goryachev, H. Miao, Y. Chen, Y. Ma, D. Mason, M. Rossi, C. D. Blair, L. Ju, D. G. Blair, A. Schliesser, M. E. Tobar, and C. Zhao, Gravitational wave detectors with broadband high frequency sensitivity (2020), arXiv:2007.08766 [physics.optics].

[28] X. Li, J. Smetana, A. S. Ubhi, J. Bentley, Y. Chen, Y. Ma, H. Miao, and D. Martynov, *Phys. Rev. D* **103**, 122001 (2021).

[29] M. Korobko, Y. Ma, Y. Chen, and R. Schnabel, Light: Science & Applications **8**, 1 (2019).

[30] J. Mizuno, K. Strain, P. Nelson, J. Chen, R. Schilling, A. Rüdiger, W. Winkler, and K. Danzmann, *Physics Letters A* **175**, 273 (1993).

[31] H. Miao, N. D. Smith, and M. Evans, *Phys. Rev. X* **9**, 011053 (2019).

[32] T. Zhang, J. Bentley, and H. Miao, *Galaxies* **9**, 10.3390/galaxies9010003 (2021).

[33] T. Zhang, D. Martynov, H. Miao, and S. Danilishin, *Phys. Rev. D* **104**, 122003 (2021).

[34] T. Zhang, J. Smetana, Y. Chen, J. Bentley, D. Martynov, H. Miao, W. E. East, and H. Yang, *Phys. Rev. D* **103**, 044063 (2021), arXiv:2011.06705 [gr-qc].

[35] M. Rakhmanov, J. D. Romano, and J. T. Whelan, *Classical and Quantum Gravity* **25**, 184017 (2008).

[36] M. Rakhmanov, *Classical and Quantum Gravity* **26**, 155010 (2009).

[37] R. Essick, S. Vitale, and M. Evans, *Phys. Rev. D* **96**, 084004 (2017).

[38] If the resonator is pumped from one port, the power at the two ETMs will be imbalanced and causes speed meter response for the differential mode [? ].

[39] J. Aasi, B. P. Abbott, R. Abbott, T. Abbott, et al., *Classical and Quantum Gravity* **32**, 074001 (2015).

[40] L. Barsotti, L. McCuller, M. Evans, and P. Fritschel, *LIGO Document T1800042* (2018).

[41] S. Hild, M. Abernathy, F. Acernese, P. Amaro-Seoane, N. Andersson, K. Arun, F. Barone, B. Barr, M. Barsuglia, M. Beker, N. Beveridge, S. Birindelli, S. Bose, L. Bosi, S. Braccini, C. Bradaschia, T. Bulik, E. Calloni, G. Cella, E. C. Mottin, S. Chelkowski, A. Chinaccini, J. Clark, E. Coccia, C. Colacino, J. Colas, A. Cumming, L. Cunningham, E. Cuoco, S. Danilishin, K. Danzmann, R. D. Salvo, T. Dent, R. D. Rosa, L. D. Fiore, A. D. Virgilio, M. Doets, V. Fafone, P. Falferi, R. Flaminio, J. Franc, F. Frasconi, A. Freise, D. Friedrich, P. Fulda, J. Gair, G. Gemme, E. Genin, A. Gennai, A. Giazotto, K. Glampedakis, C. Gräf, M. Granata, H. Grote, G. Guidi, A. Gurkovsky, G. Hammond, M. Hannam, J. Harms, D. Heinert, M. Hendry, I. Heng, E. Hennes, J. Hough, S. Husa, S. Huttner, G. Jones, F. Khalili, K. Kokeyama, K. Kokkotas, B. Krishnan, T. G. F. Li, M. Lorenzini, H. Lück, E. Ma-  
jorana, I. Mandel, V. Mandic, M. Mantovani, I. Martin, C. Michel, Y. Minenkov, N. Morgado, S. Mosca, B. Mours, H. Müller-Ebhardt, P. Murray, R. Nawrodt, J. Nelson, R. Oshaughnessy, C. D. Ott, C. Palomba, A. Paoli, G. Parguez, A. Pasqualetti, R. Passaquieti, D. Passuello, L. Pinard, W. Plastino, R. Poggiani, P. Popolizio, M. Prato, M. Punturo, P. Puppo, D. Rabeling, P. Rapagnani, J. Read, T. Regimbau, H. Rehbein, S. Reid, F. Ricci, F. Richard, A. Rocchi, S. Rowan, A. Rüdiger, L. Santamaría, B. Sassolas, B. Sathyaprakash, R. Schnabel, C. Schwarz, P. Seidel, A. Sintes, K. Somiya, F. Speirits, K. Strain, S. Stargin, P. Sutton, S. Tarabrin, A. Thüring, J. van den Brand, M. van Veggel, C. van den Broeck, A. Vecchio, J. Veitch, F. Vetrano, A. Vicere, S. Vyatchanin, B. Willke, G. Woan, and K. Yamamoto, *Classical and Quantum Gravity* **28**, 094013 (2011).

[42] M. Evans, R. X. Adhikari, C. Afie, S. W. Ballmer, S. Biscoveanu, S. Borhanian, D. A. Brown, Y. Chen, R. Eisenstein, A. Gruson, et al., arXiv preprint arXiv:2109.09882 (2021).

[43] V. Srivastava, D. Davis, K. Kuns, P. Landry, S. Ballmer, M. Evans, E. D. Hall, J. Read, and B. S. Sathyaprakash, *Astrophys. J.* **931**, 22 (2022), arXiv:2201.10668 [gr-qc].

[44] J.-Y. Vinet, B. Meers, C. N. Man, and A. Brillet, *Phys. Rev. D* **38**, 433 (1988).

[45] B. J. Meers, *Phys. Rev. D* **38**, 2317 (1988).

[46] T. Akutsu, S. Kawamura, A. Nishizawa, K. Arai, K. Yamamoto, D. Tatsumi, S. Nagano, E. Nishida, T. Chiba, R. Takahashi, N. Sugiyama, M. Fukushima, T. Yamazaki, and M.-K. Fujimoto, *Phys. Rev. Lett.* **101**, 101101 (2008).

[47] A. Nishizawa, S. Kawamura, T. Akutsu, K. Arai, K. Yamamoto, D. Tatsumi, E. Nishida, M.-a. Sakagami, T. Chiba, R. Takahashi, and N. Sugiyama, *Phys. Rev. D* **77**, 022002 (2008).

[48] F. Acernese, M. Agathos, K. Agatsuma, D. Aisa, N. Allemandou, A. Allocca, J. Amarni, P. Astone, et al., *Classical and Quantum Gravity* **32**, 024001 (2014).

[49] A. F. Brooks, G. Vajente, H. Yamamoto, R. Abbott, C. Adams, R. X. Adhikari, A. Ananyeva, S. Appert, K. Arai, J. S. Areeda, Y. Asali, S. M. Aston, C. Austin, A. M. Baer, M. Ball, S. W. Ballmer, S. Banagiri, D. Barker, L. Barsotti, J. Bartlett, B. K. Berger, J. Bettzwieser, D. Bhattacharjee, G. Billingsley, S. Biscans, C. D. Blair, R. M. Blair, N. Bode, P. Booker, R. Bork, A. Bramley, D. D. Brown, A. Buikema, C. Cahillane, K. C. Cannon, H. T. Cao, X. Chen, A. A. Ciobanu, F. Clara, C. Compton, S. J. Cooper, K. R. Corley, S. T. Countryman, P. B. Covas, D. C. Coyne, L. E. Datrier, D. Davis, C. D. Difronzo, K. L. Dooley, J. C. Driggers, P. Dupej, S. E. Dwyer, A. Effler, T. Etzel, M. Evans, T. M. Evans, J. Feicht, A. Fernandez-Galiana, P. Fritschel, V. V. Frolov, P. Fulda, M. Fyffe, J. A. Giaime, D. D. Giardina, P. Godwin, E. Goetz, S. Gras, C. Gray, R. Gray, A. C. Green, A. Gupta, E. K. Gustafson, D. Gustafson, E. Hall, J. Hanks, J. Hanson, T. Hardwick, R. K. Hasskew, M. C. Heintze, A. F. Helmling-Cornell, N. A. Holland, K. Izmui, W. Jia, J. D. Jones, S. Kandhasamy, S. Karki, M. Kasprzack, K. Kawabe, N. Kijbunchoo, P. J. King, J. S. Kissel, R. Kumar, M. Landry, B. B. Lane, B. Lantz, M. Laxen, Y. K. Lecoeuche, J. Leviton, L. Jian, M. Lormand, A. P. Lundgren, R. Macas, M. Macinnis, D. M. Macleod,

G. L. Mansell, S. Marka, Z. Marka, D. V. Martynov, K. Mason, T. J. Massinger, F. Matichard, N. Mavalvala, R. McCarthy, D. E. McClelland, S. McCormick, L. McCuller, J. McIver, T. McRae, G. Mendell, K. Merfeld, E. L. Merilh, F. Meylahn, T. Mistry, R. Mittleman, G. Moreno, C. M. Mow-Lowry, S. Mozzon, A. Mullavey, T. J. Nelson, P. Nguyen, L. K. Nuttall, J. Oberling, R. J. Oram, C. Ostheder, D. J. Ottaway, H. Overmier, J. R. Palamos, W. Parker, E. Payne, A. Pele, R. Penhorwood, C. J. Perez, M. Pirello, H. Radkins, K. E. Ramirez, J. W. Richardson, K. Riles, N. A. Robertson, J. G. Rollins, C. L. Romel, J. H. Romie, M. P. Ross, K. Ryan, T. Sadecki, E. J. Sanchez, L. E. Sanchez, S. R. Tirupatturajamanikkam, R. L. Savage, D. Schaetzl, R. Schnabel, R. M. Schofield, E. Schwartz, D. Sellers, T. Shaffer, D. Sigg, B. J. Slagmolen, J. R. Smith, S. Soni, B. Sorazu, A. P. Spencer, K. A. Strain, L. Sun, M. J. Szczepanczyk, M. Thomas, P. Thomas, K. A. Thorne, K. Toland, C. I. Torrie, G. Traylor, M. Tse, A. L. Urban, G. Valdes, D. C. Vander-Hyde, P. J. Veitch, K. Venkateswara, G. Vengopal, A. D. Viets, T. Vo, C. Vorvick, M. Wade, R. L. Ward, J. Warner, B. Weaver, R. Weiss, C. Whittle, B. Willke, C. C. Wipf, L. Xiao, H. Yu, H. Yu, L. Zhang, M. E. Zucker, and J. Zweizig, [Appl. Opt. \*\*60\*\*, 4047 \(2021\)](#).

[50] M. Evans, S. Gras, P. Fritschel, J. Miller, L. Barsotti, D. Martynov, A. Brooks, D. Coyne, R. Abbott, R. X. Adhikari, K. Arai, R. Bork, B. Kells, J. Rollins, N. Smith-Lefebvre, G. Vajente, H. Yamamoto, C. Adams, S. Aston, J. Betzweiser, V. Frolov, A. Mullavey, A. Pele, J. Romie, M. Thomas, K. Thorne, S. Dwyer, K. Izumi, K. Kawabe, D. Sigg, R. Derosa, A. Effler, K. Kokeyama, S. Ballmer, T. J. Massinger, A. Staley, M. Heinze, C. Mueller, H. Grote, R. Ward, E. King, D. Blair, L. Ju, and C. Zhao, [Phys. Rev. Lett. \*\*114\*\*, 161102 \(2015\)](#).

[51] Y. T. Liu and K. S. Thorne, [Phys. Rev. D \*\*62\*\*, 122002 \(2000\)](#).

[52] A. F. Brooks, B. Abbott, M. A. Arain, G. Ciani, A. Cole, G. Grabeel, E. Gustafson, C. Guido, M. Heintze, A. Heptonstall, M. Jacobson, W. Kim, E. King, A. Lynch, S. O'Connor, D. Ottaway, K. Mailand, G. Mueller, J. Munch, V. Sannibale, Z. Shao, M. Smith, P. Veitch, T. Vo, C. Vorvick, and P. Willem, [Appl. Opt. \*\*55\*\*, 8256 \(2016\)](#).

[53] J. G. Rollins, E. Hall, C. Wipf, and L. McCuller, Astrophysics Source Code Library, ascl (2020).

[54] H. J. Kimble, Y. Levin, A. B. Matsko, K. S. Thorne, and S. P. Vyatchanin, [Phys. Rev. D \*\*65\*\*, 022002 \(2001\)](#).

[55] M. Tse, H. Yu, N. Kijbunchoo, A. Fernandez-Galiana, P. Dupej, L. Barsotti, C. D. Blair, D. D. Brown, S. E. Dwyer, A. Effler, M. Evans, P. Fritschel, V. V. Frolov, A. C. Green, G. L. Mansell, F. Matichard, N. Mavalvala, D. E. McClelland, L. McCuller, T. McRae, J. Miller, A. Mullavey, E. Oelker, I. Y. Phinney, D. Sigg, B. J. J. Slagmolen, T. Vo, R. L. Ward, C. Whittle, R. Abbott, C. Adams, R. X. Adhikari, A. Ananyeva, S. Apertet, K. Arai, J. S. Areeda, Y. Asali, S. M. Aston, C. Austin, A. M. Baer, M. Ball, S. W. Ballmer, S. Banagiri, D. Barker, J. Bartlett, B. K. Berger, J. Bettzwieser, D. Bhattacharjee, G. Billingsley, S. Biscans, R. M. Blair, N. Bode, P. Booker, R. Bork, A. Bramley, A. F. Brooks, A. Buikema, C. Cahillane, K. C. Cannon, X. Chen, A. A. Ciobanu, F. Clara, S. J. Cooper, K. R. Corley, S. T. Countryman, P. B. Covas, D. C. Coyne, L. E. H. Datrier, D. Davis, C. Di Fronzo, J. C. Driggers, T. Etzel, T. M. Evans, J. Feicht, P. Fulda, M. Fyffe, J. A. Giaime, K. D. Giardina, P. Godwin, E. Goetz, S. Gras, C. Gray, R. Gray, A. Gupta, E. K. Gustafson, R. Gustafson, J. Hanks, J. Hanson, T. Hardwick, R. K. Hasskew, M. C. Heintze, A. F. Helmling-Cornell, N. A. Holland, J. D. Jones, S. Kandhasamy, S. Karki, M. Kasprzack, K. Kawabe, P. J. King, J. S. Kissel, R. Kumar, M. Landry, B. B. Lane, B. Lantz, M. Laxen, Y. K. Lecoeuche, J. Leviton, J. Liu, M. Lormand, A. P. Lundgren, R. Macas, M. MacInnis, D. M. Macleod, S. Márka, Z. Márka, D. V. Martynov, K. Mason, T. J. Massinger, R. McCarthy, S. McCormick, J. McIver, G. Mendell, K. Merfeld, E. L. Merilh, F. Meylahn, T. Mistry, R. Mittleman, G. Moreno, C. M. Mow-Lowry, S. Mozzon, T. J. N. Nelson, P. Nguyen, L. K. Nuttall, J. Oberling, R. J. Oram, B. O'Reilly, C. Ostheder, D. J. Ottaway, H. Overmier, J. R. Palamos, W. Parker, E. Payne, A. Pele, C. J. Perez, M. Pirello, H. Radkins, K. E. Ramirez, J. W. Richardson, K. Riles, N. A. Robertson, J. G. Rollins, C. L. Romel, J. H. Romie, M. P. Ross, K. Ryan, T. Sadecki, E. J. Sanchez, L. E. Sanchez, T. R. Saravanan, R. L. Savage, D. Schaetzl, R. Schnabel, R. M. S. Schofield, E. Schwartz, D. Sellers, T. J. Shaffer, J. R. Smith, S. Soni, B. Sorazu, A. P. Spencer, K. A. Strain, L. Sun, M. J. Szczepańczyk, M. Thomas, P. Thomas, K. A. Thorne, K. Toland, C. I. Torrie, G. Traylor, A. L. Urban, G. Vajente, G. Valdes, D. C. Vander-Hyde, P. J. Veitch, K. Venkateswara, G. Vengopal, A. D. Viets, C. Vorvick, M. Wade, J. Warner, B. Weaver, R. Weiss, B. Willke, C. C. Wipf, L. Xiao, H. Yamamoto, M. J. Yap, H. Yu, L. Zhang, M. E. Zucker, and J. Zweizig, [Phys. Rev. Lett. \*\*123\*\*, 231107 \(2019\)](#).

[56] E. D. Hall, K. Kuns, J. R. Smith, Y. Bai, C. Wipf, S. Biscans, R. X. Adhikari, K. Arai, S. Ballmer, L. Barsotti, Y. Chen, M. Evans, P. Fritschel, J. Harms, B. Kamai, J. G. Rollins, D. Shoemaker, B. J. J. Slagmolen, R. Weiss, and H. Yamamoto, [Phys. Rev. D \*\*103\*\*, 122004 \(2021\)](#).

[57] S. M. Aston, M. A. Barton, A. S. Bell, N. Beveridge, B. Bland, A. J. Brummitt, G. Cagnoli, C. A. Cantley, L. Carbone, A. V. Cumming, L. Cunningham, R. M. Cutler, R. J. S. Greenhalgh, G. D. Hammond, K. Haughian, T. M. Hayler, A. Heptonstall, J. Heefner, D. Hoyland, J. Hough, R. Jones, J. S. Kissel, R. Kumar, N. A. Lockerbie, D. Lodhia, I. W. Martin, P. G. Murray, J. O'Dell, M. V. Plissi, S. Reid, J. Romie, N. A. Robertson, S. Rowan, B. Shapiro, C. C. Speake, K. A. Strain, K. V. Tokmakov, C. Torrie, A. A. van Veggel, A. Vecchio, and I. Wilmot, [Classical and Quantum Gravity \*\*29\*\*, 235004 \(2012\)](#).

[58] Z. Michael and S. Whitcomb, [LIGO-DCC \(1997\)](#).

[59] A. Cavalleri, G. Ciani, R. Dolesi, M. Hueller, D. Nicolodi, D. Tombolato, S. Vitale, P. Wass, and W. Weber, [Physics Letters A \*\*374\*\*, 3365 \(2010\)](#).

[60] R. Dolesi, M. Hueller, D. Nicolodi, D. Tombolato, S. Vitale, P. J. Wass, W. J. Weber, M. Evans, P. Fritschel, R. Weiss, J. H. Gundlach, C. A. Hagedorn, S. Schlamming, G. Ciani, and A. Cavalleri, [Phys. Rev. D \*\*84\*\*, 063007 \(2011\)](#).

[61] V. Braginsky, M. Gorodetsky, and S. Vyatchanin, [Physics Letters A \*\*271\*\*, 303 \(2000\)](#).

[62] B. Benthem and Y. Levin, [Phys. Rev. D \*\*80\*\*, 062004 \(2009\)](#).

[63] [Optical Coatings and Thermal Noise in Precision Measurement](#) (Cambridge University Press, 2012).

[64] D. Heinert, K. Craig, H. Grote, S. Hild, H. Lück, R. Nawrodt, D. A. Simakov, D. V. Vasilyev, S. P. Vyatchanin, and H. Wittel, *Phys. Rev. D* **90**, 042001 (2014).

[65] J. R. Sanders and S. W. Ballmer, *Classical and Quantum Gravity* **34**, 025003 (2016).

[66] M. Maggiore, C. V. D. Broeck, N. Bartolo, E. Belgacem, D. Bertacca, M. A. Bizouard, M. Branchesi, S. Clesse, S. Foffa, J. García-Bellido, S. Grimm, J. Harms, T. Hinderer, S. Matarrese, C. Palomba, M. Peloso, A. Ricciardone, and M. Sakellariadou, *Journal of Cosmology and Astroparticle Physics* **2020** (03), 050.

[67] B. P. Abbott et al. (LIGO Scientific, Virgo), *Phys. Rev. D* **100**, 104036 (2019), arXiv:1903.04467 [gr-qc].

[68] R. Abbott et al. (LIGO Scientific, Virgo), *Phys. Rev. D* **103**, 122002 (2021), arXiv:2010.14529 [gr-qc].

[69] R. Abbott et al. (LIGO Scientific, VIRGO, KAGRA), arXiv preprint arXiv:2112.06861 (2021), arXiv:2112.06861 [gr-qc].

[70] E. Berti, K. Yagi, H. Yang, and N. Yunes, *Gen. Rel. Grav.* **50**, 49 (2018), arXiv:1801.03587 [gr-qc].

[71] A. Bauswein and H. T. Janka, *Phys. Rev. Lett.* **108**, 011101 (2012), arXiv:1106.1616 [astro-ph.SR].

[72] A. Bauswein, H. T. Janka, K. Hebeler, and A. Schwenk, *Phys. Rev. D* **86**, 063001 (2012), arXiv:1204.1888 [astro-ph.SR].

[73] K. Hotokezaka, K. Kiuchi, K. Kyutoku, T. Muranushi, Y.-i. Sekiguchi, M. Shibata, and K. Taniguchi, *Phys. Rev. D* **88**, 044026 (2013), arXiv:1307.5888 [astro-ph.HE].

[74] K. Takami, L. Rezzolla, and L. Baiotti, *Phys. Rev. Lett.* **113**, 091104 (2014), arXiv:1403.5672 [gr-qc].

[75] V. Paschalidis, *Class. Quant. Grav.* **34**, 084002 (2017), arXiv:1611.01519 [astro-ph.HE].

[76] B. D. Metzger, E. Quataert, and T. A. Thompson, *Mon. Not. Roy. Astron. Soc.* **385**, 1455 (2008), arXiv:0712.1233 [astro-ph].

[77] N. Bucciantini, B. D. Metzger, T. A. Thompson, and E. Quataert, *Mon. Not. Roy. Astron. Soc.* **419**, 1537 (2012), arXiv:1106.4668 [astro-ph.HE].

[78] A. Bauswein, N.-U. F. Bastian, D. B. Blaschke, K. Chatzioannou, J. A. Clark, T. Fischer, and M. Oertel, *Phys. Rev. Lett.* **122**, 061102 (2019), arXiv:1809.01116 [astro-ph.HE].

[79] M. Breschi, S. Bernuzzi, D. Godzieba, A. Perego, and D. Radice, *Phys. Rev. Lett.* **128**, 161102 (2022).

[80] A. W. Steiner, M. Hempel, and T. Fischer, *Astrophys. J.* **774**, 17 (2013), arXiv:1207.2184 [astro-ph.SR].

[81] P.-G. Reinhard and H. Flocard, *Nuclear Physics A* **584**, 467 (1995).

[82] A. Akmal, V. R. Pandharipande, and D. G. Ravenhall, *Phys. Rev. C* **58**, 1804 (1998), arXiv:nucl-th/9804027.

[83] K. Takami, L. Rezzolla, and L. Baiotti, *Phys. Rev. D* **91**, 064001 (2015), arXiv:1412.3240 [gr-qc].

[84] C. Palenzuela, S. L. Liebling, D. Neilsen, L. Lehner, O. L. Caballero, E. O'Connor, and M. Anderson, *Phys. Rev. D* **92**, 044045 (2015), arXiv:1505.01607 [gr-qc].

[85] M. Hempel, T. Fischer, J. Schaffner-Bielich, and M. Liebendorfer, *Astrophys. J.* **748**, 70 (2012), arXiv:1108.0848 [astro-ph.HE].

[86] F. Douchin and P. Haensel, *Astron. Astrophys.* **380**, 151 (2001), arXiv:astro-ph/0111092.

[87] R. Abbott et al. (LIGO Scientific, VIRGO, KAGRA), arXiv preprint arXiv:2111.03634 (2021), arXiv:2111.03634 [astro-ph.HE].

[88] T. Damour, A. Nagar, and L. Villain, *Phys. Rev. D* **85**, 123007 (2012), arXiv:1203.4352 [gr-qc].

[89] H. Miao, H. Yang, and D. Martynov, *Phys. Rev. D* **98**, 044044 (2018), arXiv:1712.07345 [gr-qc].

[90] H. Yang, V. Paschalidis, K. Yagi, L. Lehner, F. Pretorius, and N. Yunes, *Phys. Rev. D* **97**, 024049 (2018), arXiv:1707.00207 [gr-qc].

[91] W. E. East and L. Lehner, *Phys. Rev. D* **100**, 124026 (2019), arXiv:1909.07968 [gr-qc].

[92] L. Barsotti, M. Evans, and P. Fritschel, *Classical and Quantum Gravity* **27**, 084026 (2010).